Robotica (2015) volume 33, pp. 1795–1812. © Cambridge University Press 2014
doi:10.1017/S026357471400099X

Adaptive motion control of arm rehabilitation robot based on impedance identification

Aiguo Song*, Lizheng Pan, Guozheng Xu and Huijun Li

School of Instrument Science and Engineering, Southeast University, Nanjing 210096, P. R. China

(Accepted March 26, 2014. First published online: May 1, 2014)

SUMMARY

There is increasing interest in using rehabilitation robots to assist post-stroke patients during rehabilitation therapy. The motion control of the robot plays an important role in the process of functional recovery training. Due to the change of the arm impedance of the post-stroke patient in the passive recovery training, the conventional motion control based on a proportional-integral (PI) controller is difficult to produce smooth movement of the robot to track the designed trajectory set by the rehabilitation therapist. In this paper, we model the dynamics of post-stroke patient arm as an impedance model, and propose an adaptive control scheme, which consists of an adaptive PI control algorithm and an adaptive damping control algorithm, to control the rehabilitation robot moving along predefined trajectories stably and smoothly. An equivalent two-port circuit of the rehabilitation robot and human arm is built, and the passivity theory of circuits is used to analyze the stability and smoothness performance of the robot. A slide Least Mean Square with adaptive window (SLMS-AW) method is presented for on-line estimation of the parameters of the arm impedance model, which is used for adjusting the gains of the PI-damping controller. In this paper, the Barrett WAM Arm manipulator is used as the main hardware platform for the functional recovery training of the post-stroke patient. Passive recovery training has been implemented on the WAM Arm, and the experimental results demonstrate the effectiveness and potential of the proposed adaptive control strategies.

KEYWORDS: Rehabilitation robot; Stroke; Impedance model; Parameter identification; Robot control.

1. Introduction

Stroke is a leading cause of serious, long-term disability. For instance, in China every year there are about 2,000,000 people suffering from a stroke, of which approximately 66 percent survives the stroke, commonly involving deficits of motor function.[1] Although the optimal therapy for patients who suffer from stroke is still a point of discussion, one theory is that patients will recover better and faster when having intensive physiotherapy directly after the accident. According to motion and relearning theory, undamaged brain tissue will then take over the functionality of the damaged tissue, and the lost functionality caused by the stroke will be regained.[2] In recent years, there is increasing interest in using robotic devices to help provide rehabilitation therapy following neurologic injuries such as stroke and spinal cord injury.[3] In order to assist the stroke patients during rehabilitation therapy, much of this new work has focused on developing more sophisticated, many degrees-of-freedom (DOF) robot-assisted rehabilitation therapy systems, such as MIME,[4] ARM Guide,[5] MIT-MANUS,[6] and UECM.[7] And there has also been a progression in the development of control strategies that specify how these devices interact with participants.

Robotic aids can provide programmable levels of assistance, and automatically modify their output based on sensor data using control frameworks.[8,9] The goal of robotic therapy control algorithms is to control robotic devices for rehabilitation exercise, so that the robot-assisted training is helpful to the improvement of motor recovery. In clinic, rehabilitation robot usually works on two modes, one

* Corresponding author. E-mail: a.g.song@seu.edu.cn

is passive recovery training mode, another is active recovery training mode. The passive recovery training is the initial stage of rehabilitation training, and its therapy aim is to reduce the muscle tone and provoke motor spasticity, and increase impaired-limb movable region.[10] The main objective in this stage is to control the robot stably and smoothly to stretch the patient moving along a predefined trajectory with the position controller. Thus, in the passive recovery training mode, providing a desired movement trajectory with appropriate velocity to the patient is a key issue for the robot control. O'Malley *et al.* used a traditional fixed gain proportional-derivative (PD) trajectory controller to control the Rice Wrist moving along the desired trajectory in the GoTo mode and found that the performance was dependent on the selection of PD gains.[11] Erol *et al.* proposed an artificial neural network-based proportional-integral (PI) gain, scheduling direct force controller which can automatically adjust control gains for a wide range of patients with different conditions.[12] Xu and Song designed a fuzzy logic based PD position controller for upper-limb rehabilitation robot to obtain stable motion tracking performance.[13] Xu and Song then developed an adaptive impedance controller based on evolutionary dynamic fuzzy neural networks for arm rehabilitation robot to obtain the robust control performance when the change of impaired limb's physical condition happens.[14] Owing to the difficulty of neural network training and lack of sufficient training set, it is not easy to satisfy the practical need.

In this paper, a novel control scheme is proposed, which is the combination of adaptive PI control and adaptive damping control. The passivity theory is introduced to analyze the stability performance of the rehabilitation robot when interacting with patient, moreover, a slide Least Mean Squares with adaptive window (SLMS-AW) method is given to estimate the parameters of human arm impedance on-line for adjusting the gains of the PI-damping controller. The Barrett WAM Arm manipulator is used as the main hardware platform of rehabilitation robot for the functional recovery training of the post-stroke patient, and the passive recovery training has been implemented on the WAM Arm.

2. Arm Rehabilitation Robot System

Figure 1 depicts the configuration and control structure of the arm rehabilitation robot system, which consists of a robot with some DOF, PC-based controller, an arm support device at the end of the robot, a multi-dimensional force/torque sensor installed between the robot end and the arm support. During the rehabilitation training, the arm of the post-stroke patient is banded to the arm support device at the end of the robot. The robot drives the human arm to track the designed trajectory circularly under the control of PC. The position sensor measures the movement of the robot as well as the force/torque sensor measures the interactive force between the rehabilitation robot and the arm of post-stroke patient for the robot control. The control structure of position tracking can be shown as Fig. 1(b).

3. Modeling of Rehabilitation Robot System

3.1. Dynamics of the rehabilitation robot

For the simplification of the analysis, we only consider the one-DOF case of the rehabilitation robot; however, the results of the analysis are easy to expand to n-DOF cases.

The robot dynamics can be expressed as follows:

$$f_c(t) - f_h(t) = m_r\ddot{x}_r(t) + b_r\dot{x}_r(t) + k_r x_r(t), \tag{1}$$

where f_c is output of controller as a force command, x_r is displacement of the robot, and m_r, b_r, k_r denote mass, damping, and stiffness of the robot, respectively. f_h is applied force on the human arm by robot.

Equation (1) can be expressed in frequency domain by using Laplace transformation as

$$f_c(s) - f_h(s) = (m_r s + b_r + k_r/s)\dot{x}_r(s). \tag{2}$$

$$Let\, Z_r(s) = m_r s + b_r + k_r/s. \tag{3}$$

$Z_r(s)$ is mechanical impedance of the robot.

https://doi.org/10.1017/S026357471400099X Published online by Cambridge University Press

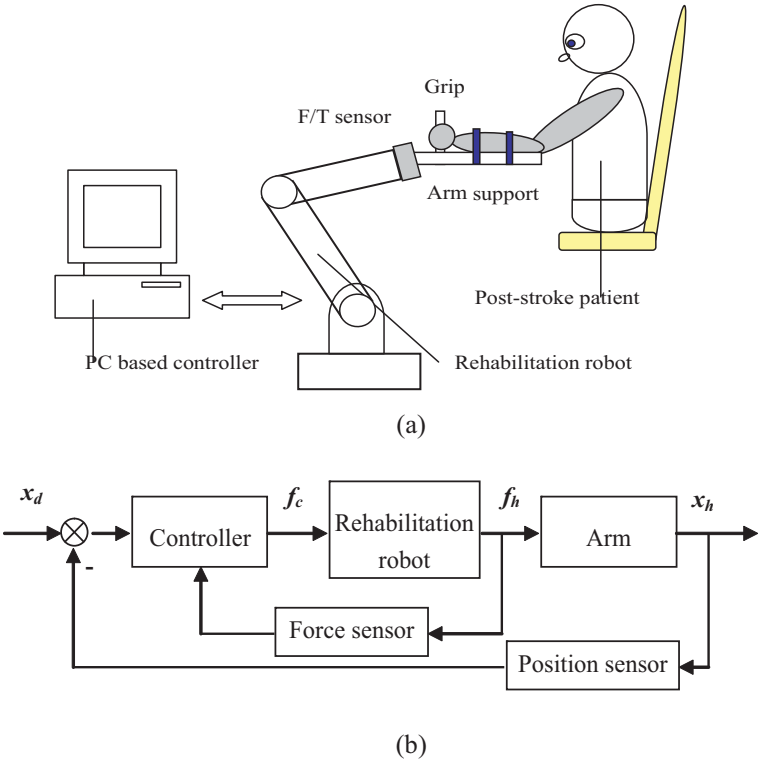

Fig. 1. Arm rehabilitation robot and control structure: (a) arm rehabilitation system; (b) control structure.

3.2. Impedance model of the human arm

The human arm dynamics is usually expressed by a mass-spring-damping system as follows:

$$f_h(t) - f_a(t) = m_h\ddot{x}_h(t) + b_h\dot{x}_h(t) + k_h x_h(t), \tag{4}$$

where f_a is the active force of the post-stoke patient. During the passive recovery training mode, f_a is sometimes caused by spastic muscle, which can be treated as an interference force affecting the rehabilitation system. x_h is displacement of the human arm, and m_h, b_h, k_h denote mass, damping, and stiffness of the human arm, respectively.

Rewriting Eq. (4) in frequency domain as

$$f_h(s) = Z_h(s)\dot{x}_h(s) + f_a(s), \tag{5}$$

$Z_h(s) = m_h s + b_h + k_h/s$, which is mechanical impedance of the human arm.

During the rehabilitation training process, owing to the changes of wrist joint, elbow joint, and shoulder joint when human arm is passively driven by the robot, the m_h, b_h, k_h are changed continuously and circularly. Thus, the mechanical impedance of the human arm is typically time-varying. Because it is impossible to pre-know the change of the $Z_h(s)$ and when the f_a is applied, the environment of rehabilitation robot is parameter uncertain.

3.3. Control of rehabilitation robot

The conventional PI controller is used for position trajectory control. In order to keep the trajectory of human arm smooth and stable without abrupt change in velocity, the damping control is incorporated with the PI control, which can prevent robot from high speed and thus maintains safety of the

https://doi.org/10.1017/S026357471400099X Published online by Cambridge University Press

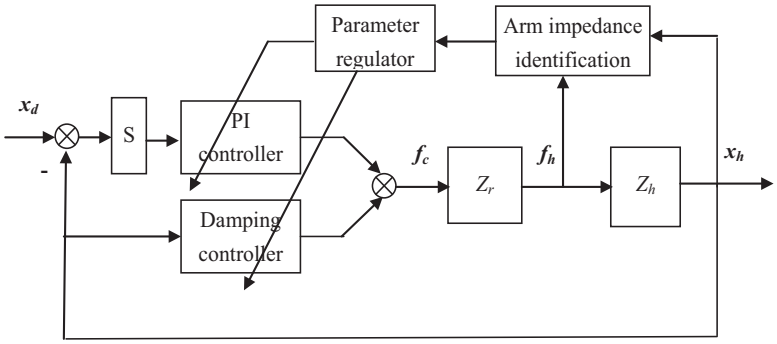

Fig. 2. Adaptive PI and damping controllers.

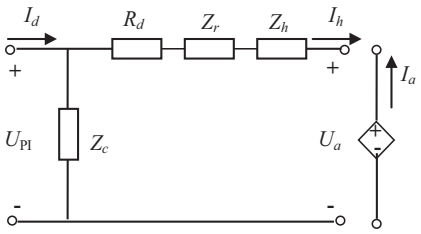

Fig. 3. Equivalent two-port circuit of arm rehabilitation robot.

rehabilitation robot system. In this paper, the block diagram of the suggested adaptive PI-damping controller is shown as Fig. 2.

The outputs of the PI control and damping control are given as the following:

$$f_{PI} = K_P(\dot{x}_d - \dot{x}_h) + K_I(x_d - x_h), \tag{6}$$

$$f_{\text{damp}} = -R_d\dot{x}_h, \tag{7}$$

$$f_c = f_{\text{PI}} + f_{\text{damp}} = K_P(\dot{x}_d - \dot{x}_h) + K_I(x_d - x_h) - R_d\dot{x}_h. \tag{8}$$

Here, K_P,K_I denote the proportional coefficient and integral coefficient of the PI controller, respectively. R_d stands for the damping coefficient which is a parameter of the damping controller.

3.4. Equivalent two-port circuit of rehabilitation robot

According to the equivalent rule between mechanical systems and electrical systems, such as current I is equivalent to velocity $\dot{x}$, and voltage U is equivalent to force F, we can express Eq. (8) in frequency domain as

$$U_c = U_{\text{PI}} + U_{\text{damp}} = Z_c(I_d - I_h) - R_dI_h, \tag{9}$$

where $Z_c(s) = K_p + K_I/s$ is defined as the control impedance of the robot. Therefore, the rehabilitation robot can be depicted as an equivalent two-port circuit based on Eqs. (1)–(9), seen in Fig. 3.

Where, for the convenience of analysis, the interference force U_a caused by patient is treated as an input voltage source of the two-port circuit, and U_a is power limited, $I_a(s) = -I_h(s)$ stands for the input velocity.

https://doi.org/10.1017/S026357471400099X Published online by Cambridge University Press

4. Analysis of Stability and Smoothness Performance

4.1. Passivity performance analysis

Definition 1:[15] An n-port circuit is said to be passive if and only if for any independent set of n-port flows, I_i injected into the circuit, and efforts, U_i applied across the circuit,

$$\int_0^\infty U^T(t)I(t)dt \geq 0, \tag{10}$$

where $U^T = [U_1, U_2, \cdots, U_n]^T \in L_2^n(R^+)$, $I^T = [I_1, I_2, \cdots, I_n]^T \in L_2^n(R^+)$.

Condition (10) is simply a statement that a passive n-port circuit may dissipate energy but cannot increase the total energy of a system in which it is an element. The passivity of the circuit implies the stability of the system.

Assumption: The parameters of robot impedance $m_r, b_r, k_r \in R^+$ are fixed, the parameters of human arm impedance $m_h, b_h, k_h \in R^+$are bounded $m_h \leq \lambda_m$, $b_h \leq \lambda_b$, $k_h \leq \lambda_k$. The parameters of controller $K_P, K_I, R_d \in R^+$ are bounded.

Let

$$Z_d(s) = R_d + Z_r + Z_h = (m_r + m_h)s + (R_d + b_r + b_h) + \frac{1}{s}(k_r + k_h). \tag{11}$$

Thus, $Z_d(s)$ is a typical energy dissipation impedance.

The relationship between effort $U(t)$ (force, voltage) and flow $I(t)$ (velocity, current) of the equivalent two-port circuit of rehabilitation robot can be conveniently specified by its hybrid matrix, $H(s)$ according to

$$\begin{bmatrix} U_{PI} \\ I_a \end{bmatrix} = \begin{bmatrix} h_{11} & h_{12} \\ h_{21} & h_{22} \end{bmatrix} \begin{bmatrix} I_d \\ U_a \end{bmatrix} = H(s) \begin{bmatrix} I_d \\ U_a \end{bmatrix}. \tag{12}$$

Deducing from Eqs. (1)–(9) and (11), we have

$$\begin{bmatrix} U_{\mathrm{PI}} \\ I_a \end{bmatrix} = \begin{bmatrix} \frac{Z_c Z_d}{Z_c+Z_d} & \frac{Z_c}{Z_c+Z_d} \\ -\frac{Z_c}{Z_c+Z_d} & \frac{1}{Z_c+Z_d} \end{bmatrix} \begin{bmatrix} I_d \\ U_a \end{bmatrix}, \tag{13}$$

$$H(s) = \begin{bmatrix} h_{11} & h_{12} \\ h_{21} & h_{22} \end{bmatrix} = \begin{bmatrix} \frac{Z_c Z_d}{Z_c+Z_d} & \frac{Z_c}{Z_c+Z_d} \\ -\frac{Z_c}{Z_c+Z_d} & \frac{1}{Z_c+Z_d} \end{bmatrix} \tag{14}$$

So, for the equivalent two-port circuit of rehabilitation robot, we have

$$\begin{aligned} \int_0^\infty [\, U_{\mathrm{PI}} \quad I_a \,] H^T [\, I_d \quad U_a \,]^T dt &= \int_0^\infty \left(h_{11} I_d^2 + (h_{12} + h_{21}) I_d U_a + h_{22} U_a^2\right) dt \\ &= \int_0^\infty \left(\frac{Z_c Z_d}{Z_c + Z_d} I_d^2 + \frac{1}{Z_c + Z_d} U_a^2\right) dt \geq 0. \end{aligned} \tag{15}$$

Therefore, the rehabilitation robot system under the PI-damping control with bounded parameters is always passive, which means it is stable.

4.2. Smooth position tracking performance analysis

Assuming the interference voltage $U_a = 0$, the movement of the human arm

$$I_h = \frac{Z_c}{Z_c + Z_d} = \frac{Z_c}{\tilde{Z}} I_d = \frac{(K_P s + K_I)}{\tilde{m}s^2 + \tilde{b}s + \tilde{k}} I_d. \tag{16}$$

https://doi.org/10.1017/S026357471400099X Published online by Cambridge University Press

Let

$$\tilde{Z} = Z_c + Z_d = (m_r + m_h)s + (R_d + b_r + b_h + K_P) + \frac{1}{s}(k_r + k_h + K_I) = \tilde{m}s + \tilde{b} + \tilde{k}/s, \quad (17)$$

where

$$\tilde{m} = m_r + m_h;\ \tilde{b} = R_d + b_r + b_h + K_P;\ \tilde{k} = k_r + k_h + K_I. \quad (18)$$

The position tracking error between the desired trajectory and real trajectory of the robot is

$$e = I_d - I_h = I_d - \frac{(K_P s + K_I)}{\tilde{m}s^2 + \tilde{b}s + \tilde{k}} I_d = \frac{\tilde{m}s^2 + (\tilde{b} - K_P)s + (\tilde{k} - K_I)}{\tilde{m}s^2 + \tilde{b}s + \tilde{k}} I_d. \quad (19)$$

Thus, the steady-state position tracking error

$$e_{\text{ss}} = \lim_{s \to 0} s e(s) \frac{1}{s} = \frac{\tilde{k} - K_I}{\tilde{k}} = \frac{k_h}{K_I + k_h}. \quad (20)$$

For an interference $f_a(t) = \delta(t)$ caused by patient, the position tracking error

$$e' = \frac{1}{\tilde{m}s^2 + \tilde{b}s + \tilde{k}} U_a. \quad (21)$$

So, the steady-state position tracking error caused by the interference U_a

$$e'_{\text{ss}} = \lim_{s \to 0} s e'(s) = 0. \quad (22)$$

The above equation means the control structure is insensitive to the interference U_a.
Let $\omega_n = \sqrt{\frac{\tilde{k}}{\tilde{m}}}$, $\zeta = \frac{1}{2}\frac{\tilde{b}}{\sqrt{\tilde{m}\tilde{k}}}$, and substitute them into Eq. (16). Then

$$G(s) = \frac{I_h}{I_d} = \frac{\frac{\omega_n^2}{\tilde{k}}(K_P s + K_I)}{s^2 + 2\zeta\omega_n s + \omega_n^2}. \quad (23)$$

From the theory of automatic control, if $\zeta \geq 1$, the control system is called damping system.

$$\tilde{b} \geq 2\sqrt{\tilde{m}\tilde{k}}. \quad (24)$$

In this case, there is no overshoot in the step response of the system, which means the smoothness performance is desired for post-stroke patient passive recovery training, so that, the parameters of the controller should satisfy the smoothness condition as

$$R_d + b_r + b_h + K_P \geq 2\sqrt{(m_r + m_h)(k_r + k_h + K_I)}. \quad (25)$$

5. Identification of Arm Impedance Model

The impaired arm's dynamics can be expressed as a time-variant mass-spring-damping model. Suppose $\hat{m}_h$, $\hat{b}_h$, $\hat{k}_h$ are estimates of m_h, b_h, k_h in Eq. (4) respectively. Then we have

$$\hat{f}_{ha} = \hat{m}_h \ddot{x}_h + \hat{b}_h \dot{x}_h + \hat{k}_h x_h, \quad (26)$$

where $f_{ha} = f_h - f_a$.

https://doi.org/10.1017/S026357471400099X Published online by Cambridge University Press

According to the Least Mean Square method

$$E = \sum_{i=1}^{N} [f_{ha}(i) - \hat{f}_{ha}(i)]^2, \tag{27}$$

$$\frac{\partial E}{\partial \hat{m}_h} = 0;\ \frac{\partial E}{\partial \hat{b}_h} = 0;\ \frac{\partial E}{\partial \hat{k}_h} = 0, \tag{28}$$

so we have

$$\begin{bmatrix} \hat{m}_h \\ \hat{b}_h \\ \hat{k}_h \end{bmatrix} = \begin{bmatrix} \sum_{i=1}^{N} \ddot{x}_h^2(i) & \sum_{i=1}^{N} \ddot{x}_h(i)\dot{x}_h(i) & \sum_{i=1}^{N} \ddot{x}_h(i)x_h(i) \\ \sum_{i=1}^{N} \dot{x}_h(i)\ddot{x}_h(i) & \sum_{i=1}^{N} \dot{x}_h^2(i) & \sum_{i=1}^{N} \dot{x}_h(i)x_h(i) \\ \sum_{i=1}^{N} x_h(i)\ddot{x}_h(i) & \sum_{i=1}^{N} x_h(i)\dot{x}_h(i) & \sum_{i=1}^{N} x_h^2(i) \end{bmatrix}^{-1} \begin{bmatrix} \sum_{i=1}^{N} \ddot{x}_h(i) f_{ha}(i) \\ \sum_{i=1}^{N} \dot{x}_h(i) f_{ha}(i) \\ \sum_{i=1}^{N} x_h(i) f_{ha}(i) \end{bmatrix}. \tag{29}$$

N is number of sampling points for parameter estimation. In order to estimate the parameters on line, we have proposed a kind of SLMS method[16] as the following:

$$\begin{bmatrix} \hat{m}_h(t) \\ \hat{b}_h(t) \\ \hat{k}_h(t) \end{bmatrix} = \begin{bmatrix} \sum_{i=t-N+1}^{t} \ddot{x}_h^2(i) & \sum_{i=t-N+1}^{t} \ddot{x}_h(i)\dot{x}_h(i) & \sum_{i=t-N+1}^{t} \ddot{x}_h(i)x_h(i) \\ \sum_{i=t-N+1}^{t} \dot{x}_h(i)\ddot{x}_h(i) & \sum_{i=t-N+1}^{t} \dot{x}_h^2(i) & \sum_{i=t-N+1}^{t} \dot{x}_h(i)x_h(i) \\ \sum_{i=t-N+1}^{t} x_h(i)\ddot{x}_h(i) & \sum_{i=t-N+1}^{t} x_h(i)\dot{x}_h(i) & \sum_{i=t-N+1}^{t} x_h^2(i) \end{bmatrix}^{-1} \times \begin{bmatrix} \sum_{i=t-N+1}^{t} \ddot{x}_h(i) f_{ha}(i) \\ \sum_{i=t-N+1}^{t} \dot{x}_h(i) f_{ha}(i) \\ \sum_{i=t-N+1}^{t} x_h(i) f_{ha}(i) \end{bmatrix}, \tag{30}$$

$$\left[\hat{Z}_h(t)\right] = [A(t)]^{-1}[C(t)] \quad t \geq N. \tag{31}$$

The elements of the matrixes [A(t)] and [C(t)] can be quickly calculated by using slide method as:

$$\begin{aligned} a_{i,j}(t+1) &= \sum_{k=t-N+2}^{t+1} x_h^{(3-i)}(k)x_h^{(3-j)}(k) \\ &= a_{i,j}(t) + x_h^{(3-i)}(t+1)x_h^{(3-j)}(t+1) - x_h^{(3-i)}(t-N+1)x_h^{(3-j)}(t-N+1); \\ &\qquad i = 1,2,3;\ j = 1,2,3, \end{aligned} \tag{32}$$

$$\begin{aligned} c_i(t+1) &= \sum_{k=t-N+2}^{t+1} x_h^{(3-i)}(k) f_{ha}(k) \\ &= c_i(t) + x_h^{(3-i)}(t+1) f_{ha}(t+1) - x_h^{(3-i)}(t-N+1) f_{ha}(t-N+1); \quad i = 1,2,3. \end{aligned} \tag{33}$$

In general, the parameter N is fixed. In this research, in order to estimate the impaired limb's parameters more effectively and real time, a SLMS-AW identification algorithm is given. N is

https://doi.org/10.1017/S026357471400099X Published online by Cambridge University Press

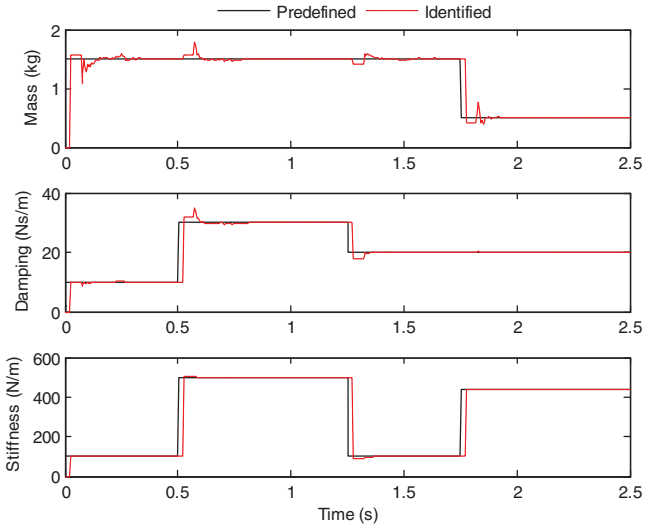

(a)

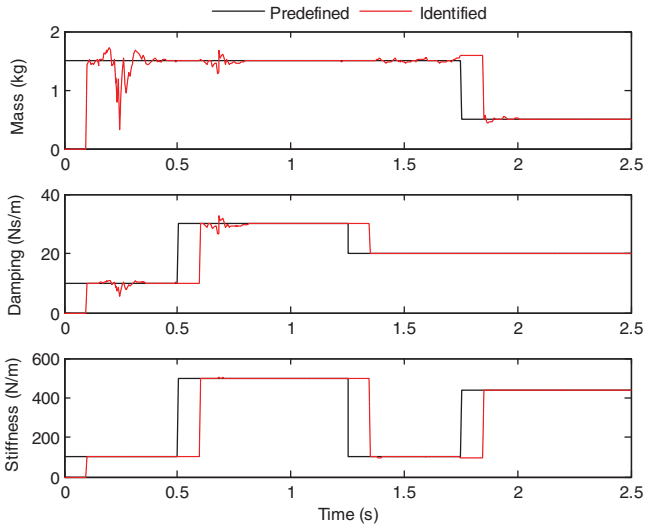

(b)

Fig. 4. Identification results of human arm impedance: (a) identification using SLMS-AW; (b) identification using traditional SLMS.

dynamically adapted according to the variations of f_{ha} and $\ddot{x}_h$, which can be expressed as:

$$N = f(\Delta\ddot{x}_h, \Delta f_{ha}), \quad N \in [N_{\min}, N_{\max}],$$
$$f(\Delta\ddot{x}_h, \Delta f_{ha}) = N_{\max} - (N_{\max} - N_{\min}) \bullet \left[(1-\lambda)\frac{\Delta\ddot{x}_h}{\Delta\ddot{x}_{\max}} + \lambda\frac{\Delta f_{ha}}{\Delta f_{\max}}\right], \tag{34}$$

where $N_{\min}$, $N_{\max}$ are the up and low limitation of N, respectively, $\Delta\ddot{x}_{\max}$and $\Delta f_{\max}$ are the maximum variations of accelerator and force, and $\lambda$is the weight coefficient.

To verify the performance of the suggested SLMS-AW, some simulation experiments have been carried out. The N for SLMS-AW is set to [10, 40]. The results of identification of mass, damping, and stiffness of human arm impedance are shown in Fig. 4. For comparison, the identification results of traditional SLMS identification algorithm are also given, in which the N is set to be 40. In Fig. 4, solid line represents the impedance parameters of human arm which are predefined according to the experimental results and clinical analysis in refs. [17] and [18], and dashed line represents the

https://doi.org/10.1017/S026357471400099X Published online by Cambridge University Press

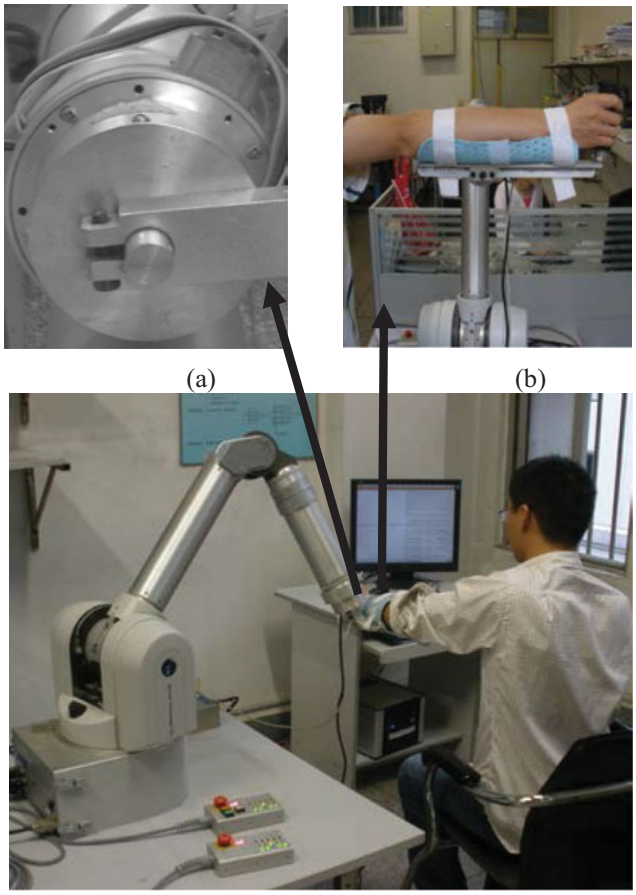

Fig. 5. Rehabilitation robot systems based on WAM Arm: (a) three-dimensional sensor; (b) Arm support device.

identification curve. From the identification results in Fig. 4, it can be concluded that the proposed SLMS-AW algorithm is obviously more accurate, robust and real-time than the traditional SLMS method.

6. Experiment

6.1. Experimental setup

The Barrett WAM Arm manipulator shown in Fig. 5 is used as the main hardware platform for the functional recovery therapy in this research. The standard WAM Arm is a 4-DOF highly dexterous, naturally back-drivable manipulator. The upper-limb rehabilitation experimental setup consists of the Barrett WAM Arm, a three-dimensional force sensor (Fig. 5(a)), an arm support device (Fig. 5(b)), and an external PC offered by Barrett. In order to record the force between the patient arm and the rehabilitation robot end-effector, a three-dimensional force sensor[19] is designed and installed at the end-effector of the WAM Arm. With the arm support device, the patient forearm can be well supported on it. An external PC running with the Linux system was responsible for running the control loop and providing high-level command of the WAM rehabilitation robot system. The control loop is the repeated reading of motor angles and commanding of motor torques at 2 KHz. Following the generated high-level command, the patient arm could be stretched by the WAM rehabilitation robot and perform various physical training.

6.2. Control system

During the robot-assisted passive recovery training, the physical state of patient's upper-limb is not ideal, there are many uncertain factors affecting the control performance, e.g. pose-position change,

https://doi.org/10.1017/S026357471400099X Published online by Cambridge University Press

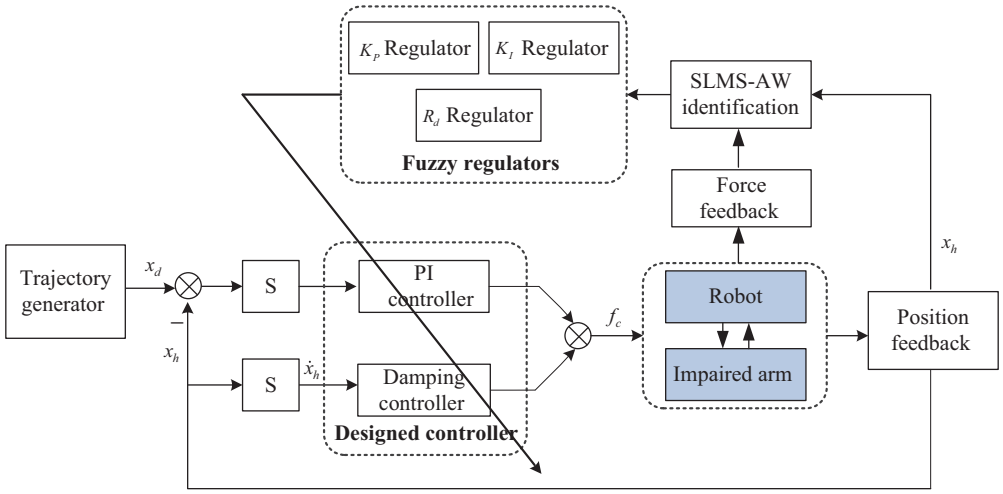

Fig. 6. Control system block diagram for passive training.

muscle spasm and tremor, even occasional cough, and other external disturbance. In this research, the adaptive PI control algorithm and damping control algorithm are proposed for the passive recovery training to control the WAM Arm stably and smoothly to stretch the impaired limb moving along the predefined trajectory. The adaptive PI-damping controller is expected to provide better performance than the traditional fixed gain PI controller because of its ability of adjusting the control gains in accordance with changes of the patient's physical state. The block diagram of proposed control strategy is given in Fig. 6.

As shown in Fig. 6, the designed control system mainly consists of controller unit, identification unit, and parameter regulators. The designed controller adopts adaptive PI-damping algorithm. In this research, damping control works as an energy-dissipation part, which is proportional to velocity with opposite direction and is incorporated with PI control. Under the designed controller, the rehabilitation robot stretches the impaired limb to do recovery training. The proposed control method can effectively prevent robot from high speed and abrupt interference caused by post-stroke patient, so that the robot always runs with stable and smooth tracking movement during rehabilitation training. The SLMS-AW identification unit estimates the impaired-limb impedance parameters online, which stand for the dynamic state of the training arm. Then the parameter regulators adjust K_P, K_I, and R_d of the designed controller according to the arm physical condition.

In this paper, fuzzy reasoning logic is adopted to adjust the controller parameters. There are three separate fuzzy regulators for theK_P, K_I, and $R_d$parts, respectively. During the rehabilitation exercise, $\hat{m}_h$,$\hat{b}_h$,$\hat{k}_h$ of the training limb are estimated by SLMS-AW identification. In order to regulate the control parameters effectively and appropriately, the identified results of mass and stiffness are used for adjusting K_P, and the identified results of mass and damping are used for adjusting K_I. For the damping control, the identified dumping and measured active force of subject are used to regulate R_d. All the inputs of fuzzy regulators are scaled to [0,1], and the corresponding outputs are separately scaled: $K_P \in [500,700]$, $K_I \in [650,900]$, $R_d \in [0,50]$. Meanwhile, during the fuzzification and defuzzification, all the inputs and outputs are defined as five fuzzy sets: small (S), small and middle (SM), middle (M), middle and large (ML), and large (L), respectively. According to the practical application, the K_P regulator should adjust gently and be less affected by the mass change, while the R_d regulator should be magnificently sensitive to the active force of subject. The designed fuzzy reasoning rules for regulating K_P, K_I, and $R_d$are shown in Tables I–III, respectively, and the corresponding input–output surface maps are shown in Figs. 7–9.

6.3. Experimental results

To verify the effectiveness of the proposed adaptive PI-damping controller, two healthy subjects are recruited to participate in the robot-aided upper-limb passive rehabilitation exercise. Figure 10 shows the sinusoidal trajectory tracking performances of the proposed adaptive PI-damping strategy

https://doi.org/10.1017/S026357471400099X Published online by Cambridge University Press

Table I. Fuzzy reasoning rules for K_P.

	k-scaled				
m-scaled	S	SM	M	ML	L
S	S	S	S	SM	M
SM	S	SM	M	M	ML
M	S	SM	M	M	ML
ML	SM	SM	M	ML	ML
L	M	M	ML	ML	L

Table II. Fuzzy reasoning rules for K_I.

	b-scaled				
m-scaled	S	SM	M	ML	L
S	S	S	SM	SM	M
SM	S	SM	SM	M	M
M	SM	SM	SM	M	ML
ML	SM	M	M	ML	ML
L	M	M	ML	ML	L

Table III. Fuzzy reasoning rules for R_d.

	b-scaled				
f-scaled	S	SM	M	ML	L
S	S	S	S	SM	SM
SM	SM	SM	SM	SM	M
M	M	M	M	M	ML
ML	ML	M	ML	ML	L
L	ML	L	L	L	L

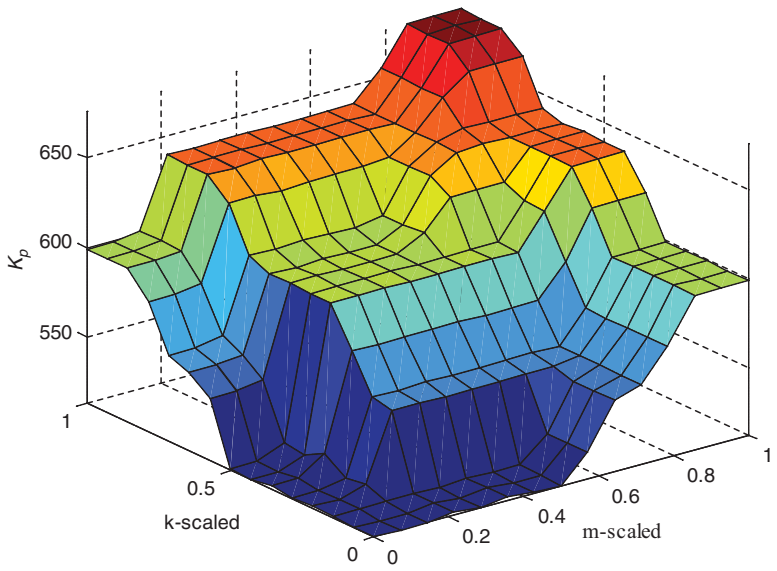

Fig. 7. Control surface of K_P.

https://doi.org/10.1017/S026357471400099X Published online by Cambridge University Press

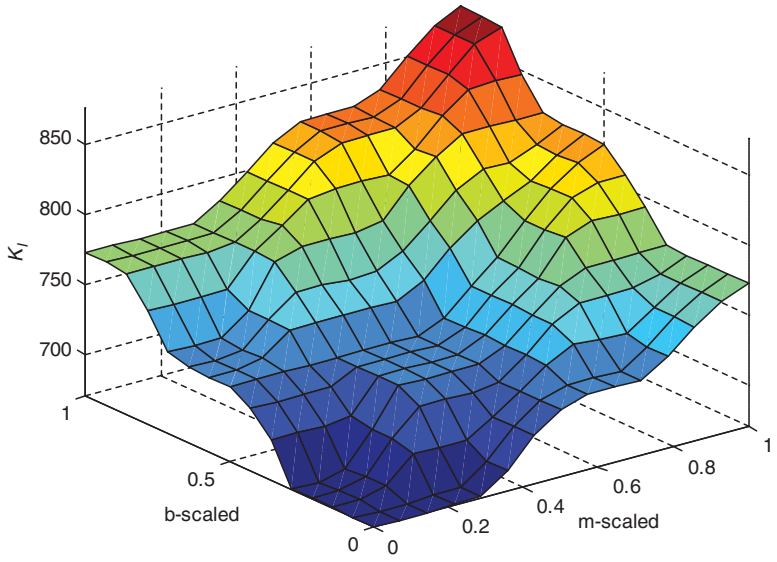

Fig. 8. Control surface of K_I.

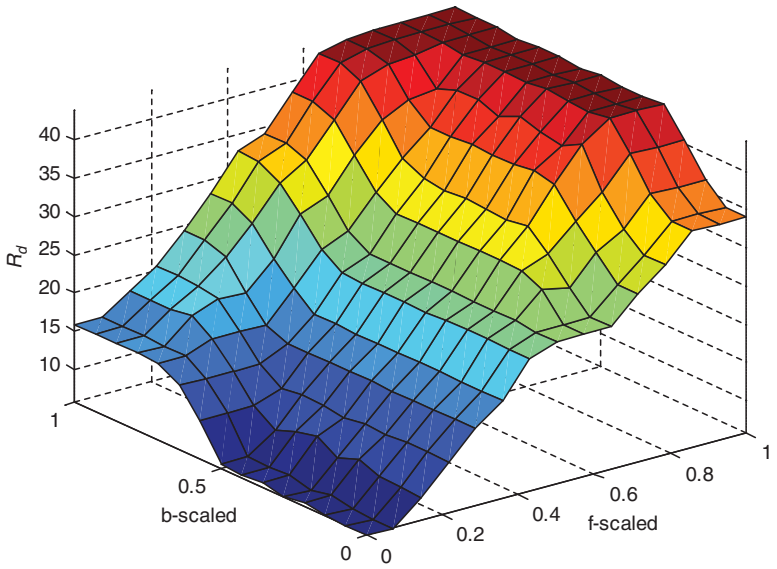

Fig. 9. Control surface of R_d.

and the traditional PI method with regard to a healthy subject sample P1 in the horizontal (J3, the 3rd joint) flexion/extension exercises. The human arm's flexion/extension limitations expressed in WAM Arm world frames are defined as –0.8 rad in flexion and 0.8 rad in extension, respectively. According to the previous experimental performances and practical application of the system, the conventional PI controller gains K_P and K_I were set as 600 and 750, respectively. The safety peak joint velocity and the maximum motor torque for four motors were set as 1.2 rad/s and 8.2 Nm, respectively. It is obvious in Fig. 10, when the participant is guided by the WAM Arm along the predefined sinusoidal trajectory, both the adaptive PI-damping controller and traditional PI controller can achieve the desired trajectories, but the tracking performance of the former is even better than that of the latter, which can be observed from the trajectory tracking error.

Meanwhile, the maximum absolute error (MAE) and sum of absolute error (SAE) of trajectory tracking are selected as two indices for quantitative evaluation of the performances of the control methods. Table IV gives the quantitative comparison results in terms of the two indices. It is shown that the MAE (0.017865) and SAE (28.446) of our methods are obviously smaller than the ones (0.049066,

https://doi.org/10.1017/S026357471400099X Published online by Cambridge University Press

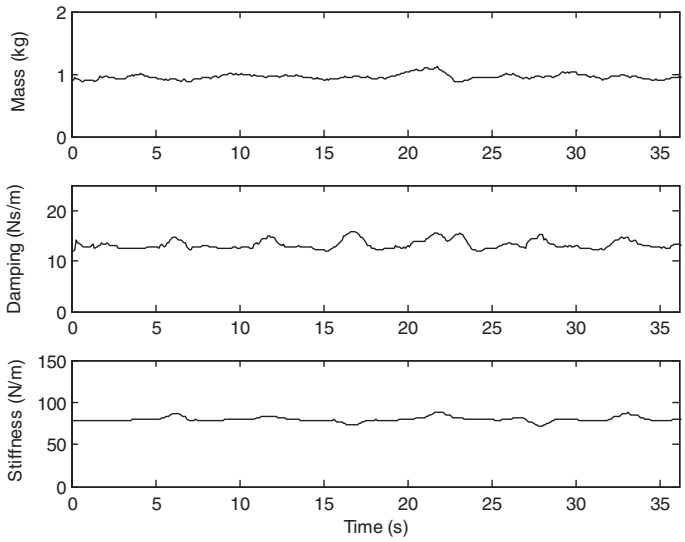

(a) Arm identification in stationary

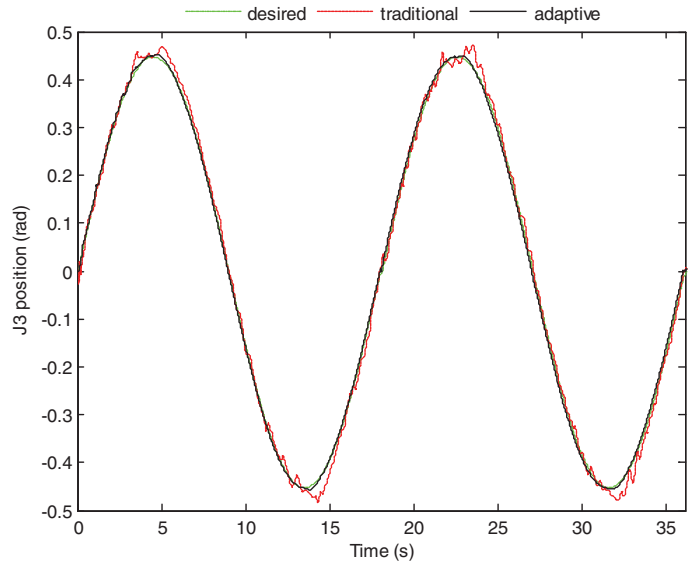

(b) Trajectory tracking in stationary

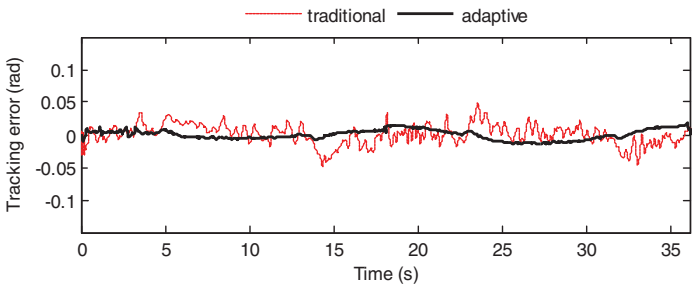

(c) Tracking error in stationary

Fig. 10. Representative results of trajectory tracking control for participant 1 (P1) in stationary state: (a) arm identification in stationary; (b) trajectory tracking in stationary; (c) tracking error in stationary.

https://doi.org/10.1017/S026357471400099X Published online by Cambridge University Press

Table IV. Control performance comparison for P1.

Tracking error (rad)		MAE	SAE
Stationary	Adaptive	0.017865	28.446
	Traditional	0.049066	44.022
Non-stationary	Adaptive	0.059341	37.835
	Traditional	0.10919	52.993

Table V. Control performance comparison for P2.

Tracking error (rad)		MAE	SAE
Stationary	Adaptive	0.015636	23.261
	Traditional	0.045019	39.651
Non-stationary	Adaptive	0.072641	38.507
	Traditional	0.10909	51.475

44.022) of the conventional method. A further comparison is made under the non-stationary condition that the participant intentionally applies disturbance force during the time interval from 10 s to 12 s. Figure 11 shows the representative results. From the human arm's impedance identification curve, when the subject is asked to apply intentional force, the estimated human arm's mass, damping, and stiffness parameters show substantial increases at the moment when the arm muscle force increases intentionally. Although a certain interference force exerts on the passive rehabilitation training system, the sinusoidal trajectory tracking of the adaptive control method is still well achieved. Moreover, it is obvious that the smoothness of the robot joint motion under the control of the adaptive PI-damping method is much better than that of the traditional PI control method, which can also be found from the MAE and SAE of trajectory tracking shown in Table IV.

To verify the adaptability of the proposed control method among different subjects, another participant P2 is asked to perform the same passive rehabilitation exercises as the one conducted for participant P1. Figures 12 and 13 show the P2's arm impedance parameter identification and trajectory tracking performance. Corresponding quantitative results in terms of the MAE and SAE are also illustrated in Table V. The quantitative analysis of trajectory tracking errors of two subjects in Tables IV and V shows that the errors of the proposed control strategy are obviously less than that of the traditional PI control method. Therefore, the experimental results demonstrate that the proposed adaptive PI-damping controller has better performance of stability, smoothness, and robustness than the conventional controller.

7. Conclusions

In this paper, an adaptive PI-damping control strategy is proposed for the rehabilitation robot motion control to realize stable and smooth recovery training of the post-stroke patient, considering that the physical condition of the training arm is usually dynamically changed during the passive recovery exercises. Impedance model of the patient arm and the equivalent two-port circuit of the rehabilitation robot together with the patient arm are built, and then the stability and smoothness performance of the robot are analyzed by using the passivity theory. Moreover, the SLMS-AW method is introduced to identify the impedance parameters of the training arm in real time, which can more effectively represent the upper-limb physical condition. Three fuzzy regulators are designed to adjust the parameters of the PI-damping controller real-time according to the current physical state of training arm. Two types of experiments with different control methods are carried out, and the experimental results demonstrate that the proposed adaptive PI-damping control strategy has better performance of stability and smoothness than the traditional PI algorithm.

https://doi.org/10.1017/S026357471400099X Published online by Cambridge University Press

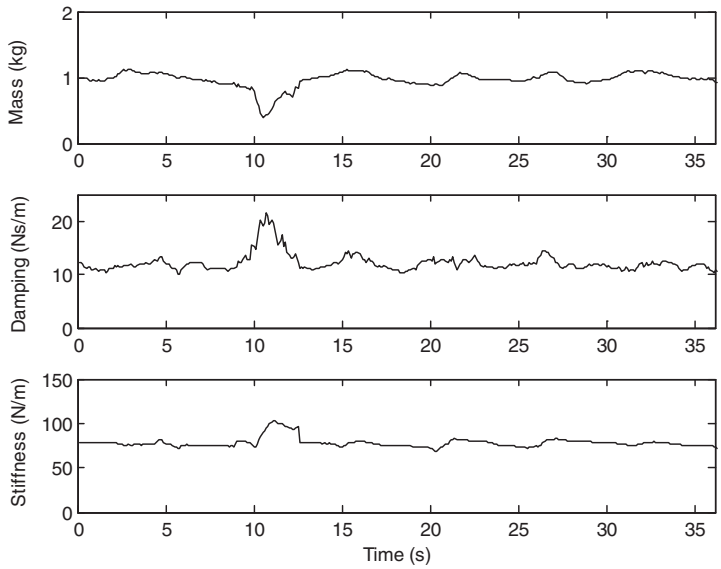

(a) Arm identification in non-stationary

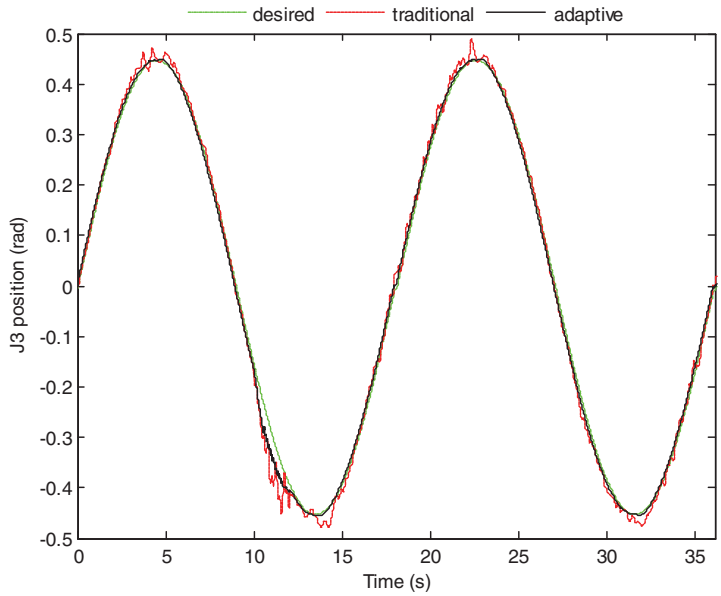

(b) Trajectory tracking in non-stationary

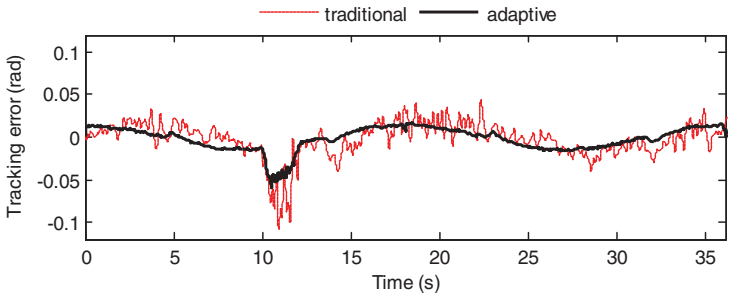

(c) Tracking error in non-stationary

Fig. 11. Representative results of trajectory tracking control for participant 1 (P1) in non-stationary state: (a) arm identification in non-stationary; (b) trajectory tracking in non-stationary; (c) tracking error in non-stationary.

https://doi.org/10.1017/S026357471400099X Published online by Cambridge University Press

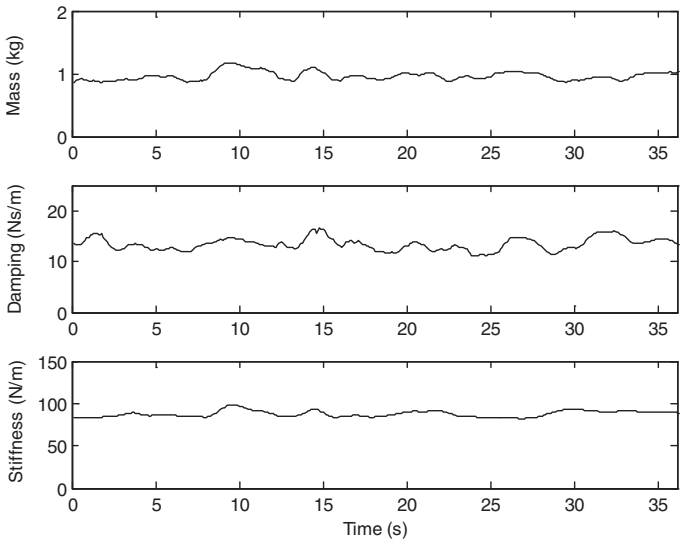

(a) Arm identification in stationary

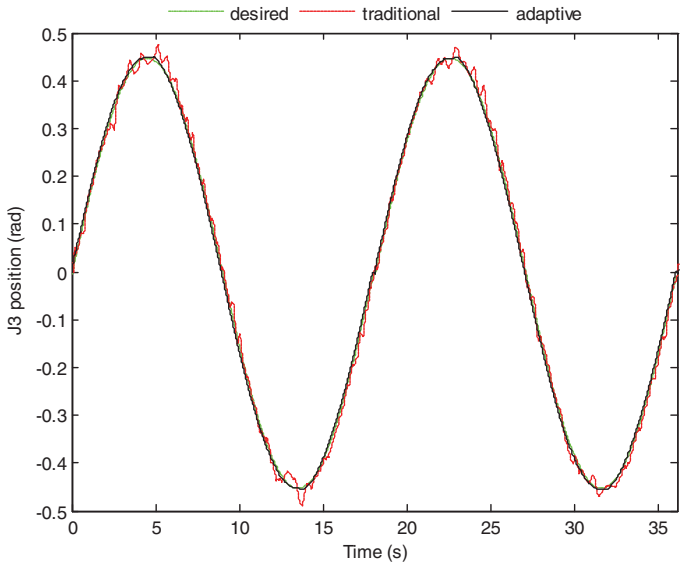

(b) Trajectory tracking in stationary

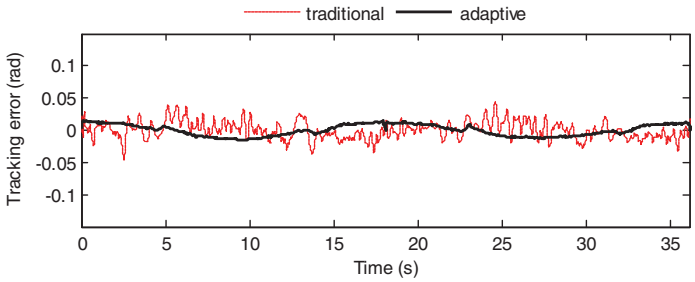

(c) Tracking error in stationary

Fig. 12. Representative results of trajectory tracking control for participant 2 (P2) in stationary state: (a) arm identification in stationary; (b) trajectory tracking in stationary; (c) tracking error in stationary.

https://doi.org/10.1017/S026357471400099X Published online by Cambridge University Press

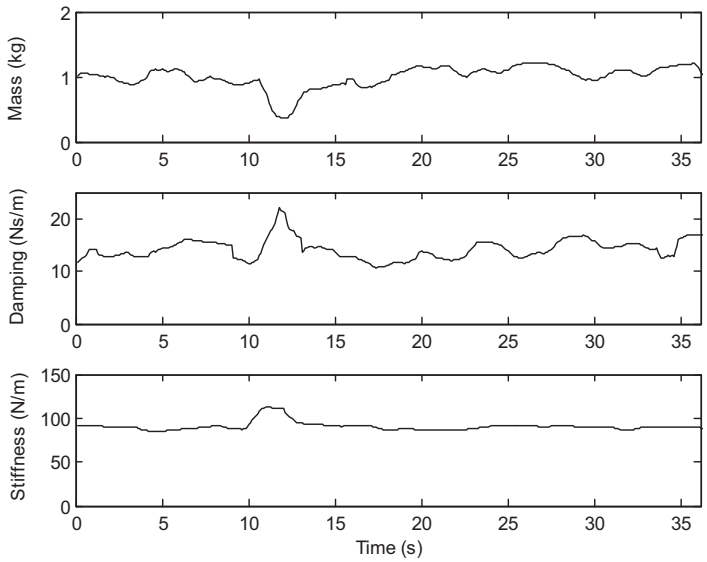

(a) Arm identification in non-stationary

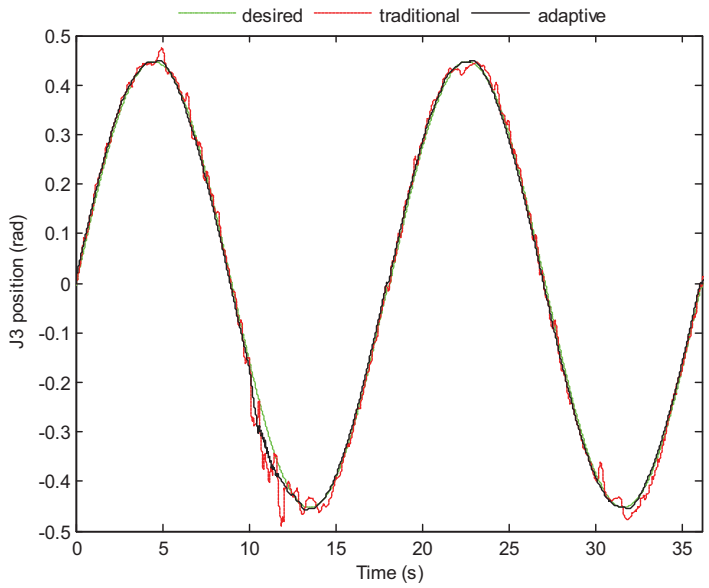

(b) Trajectory tracking in non-stationary

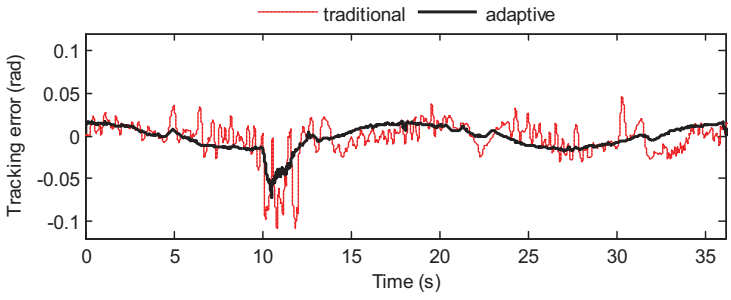

(c) Tracking error in non-stationary

Fig. 13. Representative results of trajectory tracking control for participant 2 (P2) in non-stationary state: (a) arm identification in non-stationary; (b) trajectory tracking in non-stationary; (c) tracking error in non-stationary.

https://doi.org/10.1017/S026357471400099X Published online by Cambridge University Press

Acknowledgements
The authors appreciate all colleagues in Remote Measuring and Control Laboratory, who gave valuable contributions to this work. This work was supported by the National Natural Science Foundation of China (Grant No. 61325018, 61272379, 61104206), and the Natural Science Foundation of JiangSu Province (Grant No. BK2010063). The authors would also like to thank the anonymous reviewers for their very useful comments.

References

1. Homepage of Chinese Ministry of Health, Available at http://www.moh.gov.cn/public/.
2. G. Kwakkel, B. J. Kollen and H. I. Krebs, "Effects of robot-assisted therapy on upper limb recovery after stroke: A systematic review," *Neurorehabil Neural Repair* **22**(2), 111–121 (2008).
3. M. C. Laura and J. R. David. "Review of control strategies for robotic movement training after neurologic injury," *J. NeuroEng. Rehabil*. **6**, 20 (2009).
4. P. S. Lum, C. G. Burgar, V. D. L. Machiel, P. C. Shor, M. Matra and Y. Ruth. "MIME robotic device for upper-limb neurorehabilitation in subacute stroke subjects: A follow-up study," *J. Rehabil. Res. Dev.* **43**(5), 631–642 (2006).
5. D. J. Reinkensmeyer, L. E. Kahn, M. Arerbuch, M. C. Alicia, B. D. Schmit and W. Z. Rymer. "Understanding and treating arm movement impairment after chronic brain injury: Progress with the ARM Guide," *J. Rehabil. Res. Dev*. **37**(6), 653–662 (2000).
6. H. I. Krebs, B. T. Volpe, M. L. Aisen, W. Hening, S. Adamovich, H. Poizner, K. Subrahmanyan and N. Hogan. "Robotic applications in neuromotor rehabilitation," *Robotica* **22**, 3–11 (2003).
7. Y. B. Zhang, Z. X. Wang, L. H. Ji and S. Bi, "The Clinical Application of the Upper Extremity Compound Movements Rehabilitation Training Robot," *Proceedings of the 2005 IEEE 9th International Conference on Rehabilitation Robotics*, Chicago, USA (Jun. 28–Jul. 1, 2005) pp. 91–94.
8. H. I. Krebs, N. Hogan, M. L. Aisen and B. T. Volpe, "Robot-aided neurorehabilitation," *IEEE Trans. Rehabil. Eng.* **6**, 75–87 (1998).
9. S. Eva, D. Saartje, J. P. Baeyens, R. Meeusen and K. Eric, "Effectiveness of robot-assisted gait training in persons with spinal cord injury: A systematic review," *J. Rehabil. Med.* **42**, 520–526 (2010).
10. M. Mihelj, "Human arm kinematics for robot based rehabilitation," *Robotica* **24**, 377–383 (2006).
11. M. K. O'Malley, A. Sledd, A. Gupta, V. Patoglu and J. Huegel, "The Rice Wrist: A Distal Upper Extremity Rehabilitation Robot for Stroke Therapy," *Proceedings of the IMECE*, Chicago, USA (2006) pp. 1–10.
12. E. Duygun, M. Vishnu, S. Nilanjan and T. Edward. "A New Control Approach to Robot Assisted Rehabilitation," *Proceedings of the 2005 IEEE 9th International Conference on Rehabilitation Robotics*, Chicago IL, USA (Jun. 28–Jul. 1, 2005) pp. 323–328.
13. G. Z. Xu, A. G. Song and H. J. Li, "Control system design for an upper-limb rehabilitation robot," *Adv. Robot*. **25**(1), 229–251 (2011).
14. G. Z. Xu, A. G. Song and H. J. Li, "Adaptive impedance control for upper-limb rehabilitation robot using evolutionary dynamic recurrent fuzzy neural networks," *J. Intell. Robot Syst*. **62**(2), 501–525 (2011).
15. R. J. Anderson and M. W. Spong, "Bilateral control of teleoperators with time delay," *IEEE Trans. Autom. Control* **34**(5), 494–501 (1989).
16. H. J. Li and A. G. Song, "Virtual-environment modeling and correction for force-reflecting teleoperation with time delay," *IEEE Trans. Ind. Electron.* **54**(2), 1227–1233 (2007).
17. C. C. Lin, M. S. Ju and C. W. Lin. "The pendulum test for evaluating spasticity of the elbow joint," *Arch. Phys. Med. Rehabil.* **84**, 69–74 (2003).
18. T. Noritsugu and T. Tanaka, "Application of rubber artificial muscle manipulator as a rehabilitation robot," *IEEE/ASME Trans. Mechatronics* **2**(4), 259–267 (1997).
19. A. G. Song, J. Wu, G. Qin and W. Y. Huang, "A novel self-decoupled four degree-of-freedom wrist force/torque sensor," *Measurement* **40**(9), 883–889 (2007).